JOURNAL OF MATERIALS SCIENCE 31 (1996) 3035–3042

Etching of (0 0 0 1) habit faces and matched cleavages of flux grown strontium hexaferrite crystals

URVASHI RAINA, SUSHMA BHAT, P. N. KOTRU
Department of Physics, University of Jammu, Jammu 180001, India
F. LICCI
Istituto MASPEC – CNR, Via Chiavari 18/A, 43100 Parma, Italy

Results of etching (0 0 0 1) planes of flux grown strontium hexaferrite crystals in 85% H_3PO_4 at 120 °C and 37% HCl at 100 °C are presented. Fractography reveals one-to-one correspondence of cleavage patterns on the two matched (0 0 0 1) cleaved planes. Etch patterns including hexagonal, point-bottomed pits with smooth sloping planes, hexagonal but flat-bottomed pits, geometrically centred hexagonal pits with regularly spaced terracing, eccentric hexagonal pits with irregularly spaced terracing, a large flat-bottomed hexagonal pit with a smaller point-bottomed hexagonal pit within it but having different geometrical centres and flat-bottomed pits with a beak at their centres are illustrated. It is explained that they are indicative of normal, inclined, stepped and bending dislocations in strontium hexaferrite crystals. Pits due to impurity inclusions are also explained. The explanations are supported by the results of mismatchings of etch patterns on matched cleavages.

1. Introduction

Hexagonal hard ferrites such as strontium ferrite ($SrFe_{12}O_{19}$) are interesting materials not only because they are the traditional permanent magnets but also as emerging magnetic recording media [1, 2] and as potential magneto-optical devices. The interest in hexagonal ferrites in general also stems from their possible use in electronic devices at microwave and millimetre wave frequencies [3, 4].

Studies of defect properties of technically important materials is very significant and necessary. Etching is a simple, but a very powerful, method for investigating defect structures. We have investigated the suitability of etching in the delineation of structural defects in $SrFe_{12}O_{19}$ crystals.

Crystals of $SrFe_{12}O_{19}$ were grown by the flux technique using Na_2CO_3/Bi_2O_3 as flux and the ferrite composition of about 70 mol %. In this case it is informative to note that Liu Jizhe [5] has reported etching of flux grown $PbFe_{12}O_{19}$ in 50% HCl. In this paper we report results obtained on etching of (0 0 0 1) cleavages of $SrFe_{12}O_{19}$ crystals in H_3PO_4 and HCl.

2. Experimental procedure

$SrFe_{12}O_{19}$ crystals grown by the flux method were cleaned by leaching in hot 10% HNO_3. Fresh (0 0 0 1) surfaces were obtained by cleaving the crystals by holding them tightly and then gently applying pressure over a sharp-edged knife carefully held parallel to the desired plane. The freshly obtained cleavages were then examined under a metallurgical microscope, (Neophot-2, Carl Zeiss, Germany). Etching was performed in a beaker containing 85% H_3PO_4 at 120 °C or 37% HCl at 100 °C.

3. Observations and results

3.1. Etching of (0 0 0 1) habit faces

(0 0 0 1) surfaces of $SrFe_{12}O_{19}$ when etched in 85% H_3PO_4 at 120 °C for 30 min suggest preferential etching at some isolated sites leading to hexagonal etch pits. Fig. 1 is a schematic diagram showing the structure and the orientation of the etch pits thus obtained. It is interesting to note that the types of pits include hexagonal point-bottomed with smooth sloping planes, hexagonal but flat-bottomed pits, geometrically centred hexagonal pits with regularly spaced terracing, eccentric hexagonal pits with irregularly spaced terracing, large flat-bottomed hexagonal pits with a smaller point-bottomed hexagonal pit shifted away from the geometrical centre of the former and flat-bottomed pits with a beak at their centre.

Such pit formations are indicative of normal, inclined, stepped and bending dislocations in $SrFe_{12}O_{19}$ as would be discussed in the subsequent sections of this paper. (0 0 0 1) habit faces when etched in 37% HCl for 15 min also resulted in similar types of pits.

3.2. Fractography – (0 0 0 1) cleavages

Fig. 2(a) and (b) shows a pair of matched (0 0 0 1) cleavages. One can notice the region devoid of any cleavage steps and the regions with closely spaced and

0022–2461

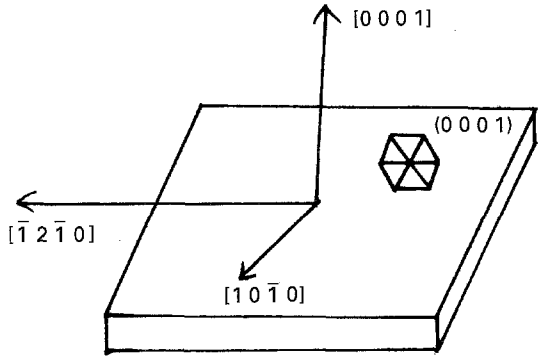

Figure 1 Schematic diagram depicting the structure and the crystallographic orientation of etch pits on (0 0 0 1) plane due to 85% H_3PO_4 at 120 °C for 30 min

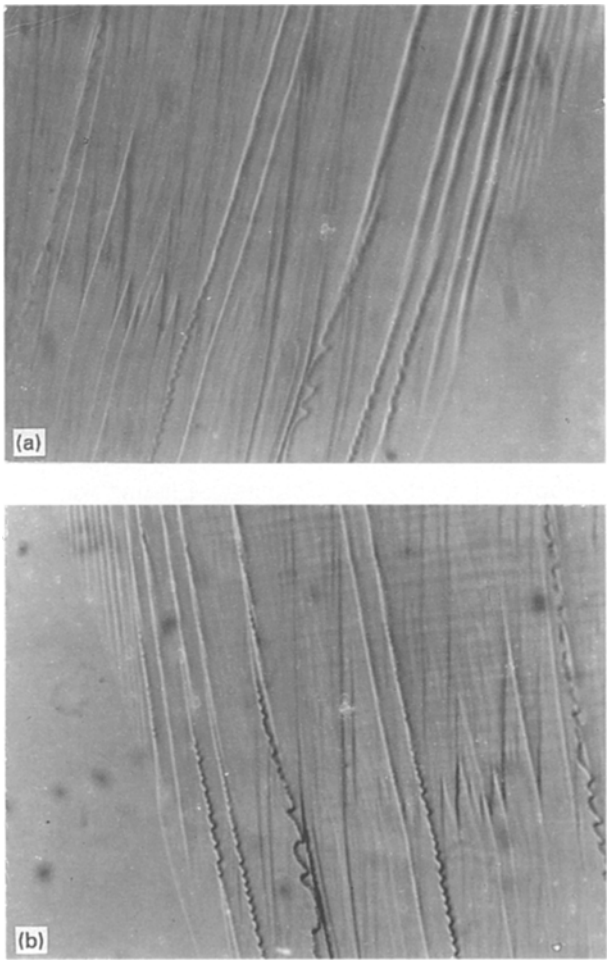

Figure 2(a, b) A pair of matched (0 0 0 1) cleavages showing plane regions as well as the regions with closely spaced and kinked cleavage steps. (× 120)

kinked cleavage steps. Fig. 3(a) and (b) illustrates (0 0 0 1) matched cleavages showing interruption in the propagation of a cleavage crack due to a fault in the crystal. Matching of the two opposite surfaces indicates deep penetration of the fault. The above illustrations showing one-to-one correspondence of the match cleaved pairs suggest perfect cleavage of the flux-grown $SrFe_{12}O_{19}$ crystals along (0 0 0 1) planes.

3.3. Etching of (0 0 0 1) cleavages

A pair of matched (0 0 0 1) cleavages when etched in 85% H_3PO_4 at 120 °C for 25 min exhibited 1:1 correspondence of point-bottomed pits whereas the flat-bottomed pits did not correspond. These results suggest the formation of point-bottomed pits due to H_3PO_4 at the sites of linear defects which could be dislocations. There can be situations where the cleavage cuts through an impurity inclusion such as to retain its divided parts on both the matched planes, as shown in a schematic diagram of Fig. 4(a, b). "C" represents the cleavage which has divided the crystal into two parts in a manner as to cut the linear defect (marked DD′) at L (see Fig. 4(a)) and the impurity inclusion at K (marked II′ in Fig. 4(b)). In this situation, if etching continues say, up to the layers 3A and 3A′ on either side of the cleavage, we expect correspondence of point-bottomed pits on matched cleaved planes at emerging points of linear defects (Fig. 4(a)) and those of flat-bottomed pits at the points of termination of impurities (Fig. 4(b)). Fig. 5(a, b) shows such a rare observation where besides, perfect correspondence between the point bottomed pits, there is a correspondence of flat bottomed pits on the two matched cleavage planes obtained on etching in H_3PO_4 at 120 °C for 25 min (see pit marked B and B′ in Fig. 5(a, b)). An impurity inclusion of such large dimensions will have a different rate of etching from that at elsewhere on the surface (say along linear defects). One can clearly notice that the flat-bottomed pits B and B′ of Fig. 5(a, b) are larger than the dislocation etch pits on both the planes. It may also be noticed that the cleavage lines of the two opposite cleavages have, on dissolution, moved in opposite directions as is expected. Sometimes such a movement of ledges interrupts the formation of a pit on encountering the specific site as has happened in the case of some point-bottomed pits on the lower right-hand corner of Fig. 5(a).

3.4. Etch patterns suggestive of inclined, stepped and bending dislocations

Spatial dislocation networks are generally present in the crystals which may involve branching and bending of dislocations inside the crystals [6–14]. During the present investigation, etching of basal planes of flux grown $SrFe_{12}O_{19}$ offered examples of hexagonal shaped smooth, point and flat-bottomed, terraced, eccentric, beaked flat-bottomed etch pits, besides a smaller pit within a large flat-bottomed pit. It also offered examples of mismatching of pits on the matched cleavage planes. All these observations are suggestive of bending, inclined and stepped dislocation lines, as explained further in the text.

3.5. Etching along grain boundaries

The grain boundary which has a grid of parallel edge dislocations along it, produces a row of equidistant point-bottomed etch pits when etched in a suitable dislocation etchant. Fig. 6(a) shows such a row of etch pits obtained on etching a (0 0 0 1) face in H_3PO_4 at 120 °C for 30 min. The row of etch pits is attributed to preferential etching of dislocations along a grain boundary.

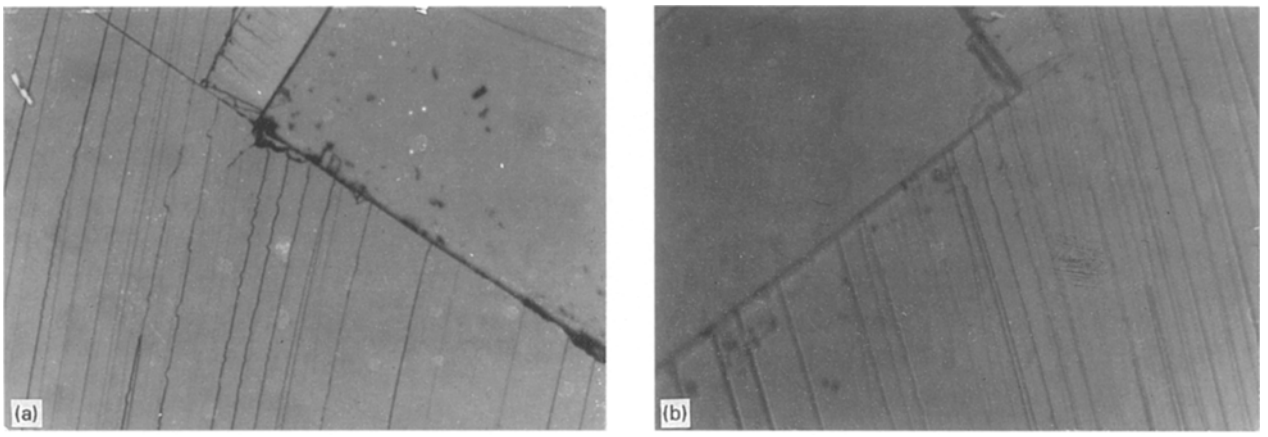

Figure 3 (a, b) (0 0 0 1) matched cleavages showing interruption in the cleavage crack propagation due to a fault. Note the exact matching. (× 120)

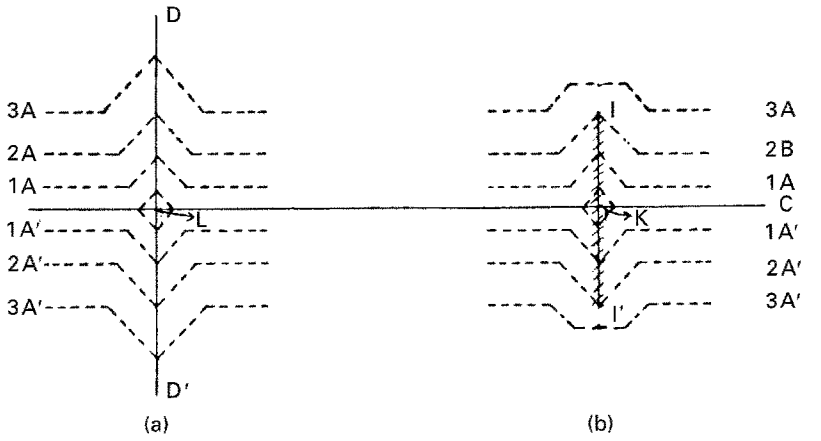

Figure 4 Schematic diagrams explaining the correspondence of point- and flat-bottomed pits on either side of the cleavage plane cutting through the linear defect at L (a) and impurity inclusion at K (b). C represents the cleavage.

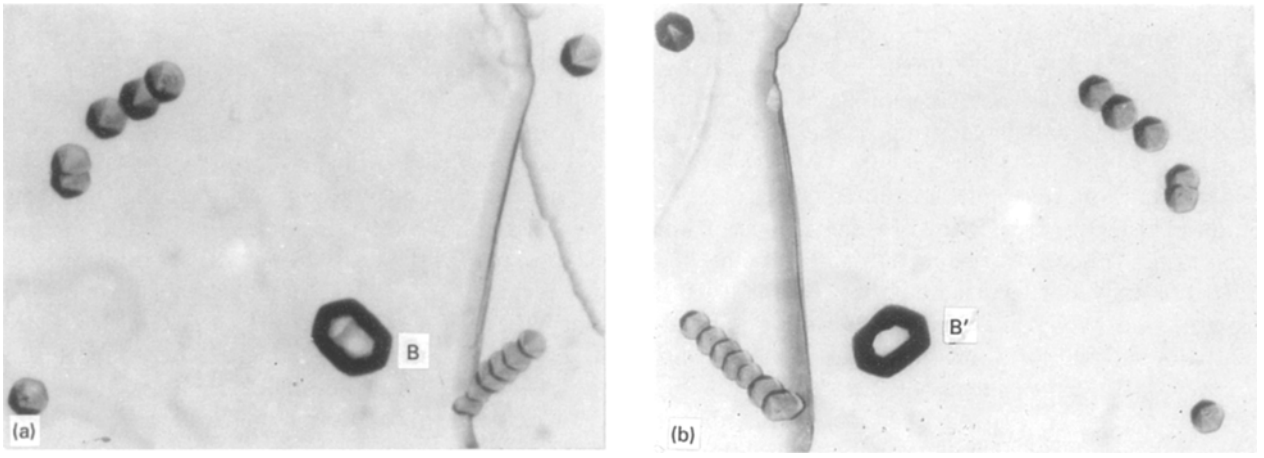

Figure 5 (a, b) Perfect correspondence between the point-bottomed and the flat-bottomed pits (B, B′) on the two matched (0 0 0 1) cleavages (etchant H_3PO_4 at 120 °C for 25 min) Note the larger dimensions of pits B and B′. (× 120)

3.6. Terraced pits

Fig. 6(a–d) are photomicrographs showing the various types of etch pit structures obtained on etching basal planes in 87% H_3PO_4 at 120 °C for 30 min. One can observe many smooth, centred point-bottomed hexagonal pits (as at E in Fig. 6(a, b, d)), smooth flat-bottomed pits (as at F in Fig. 6(d)), closely spaced, regularly terraced and centred pits (as at G in Fig. 6(a, b, d)), eccentric pits with widely spaced terracings (as at H in Fig. 6(c)), flat-bottomed and beaked hexagonal pit (as at R in Fig. 6(d)) and a small point-bottomed hexagonal pit having developed within the boundaries of a large flat-bottomed pit with its centre shifted away from the geometrical centre of the latter (as at S in Fig. 6(a, d)); notice three steps of such a formation of a large flat-bottomed pit having another

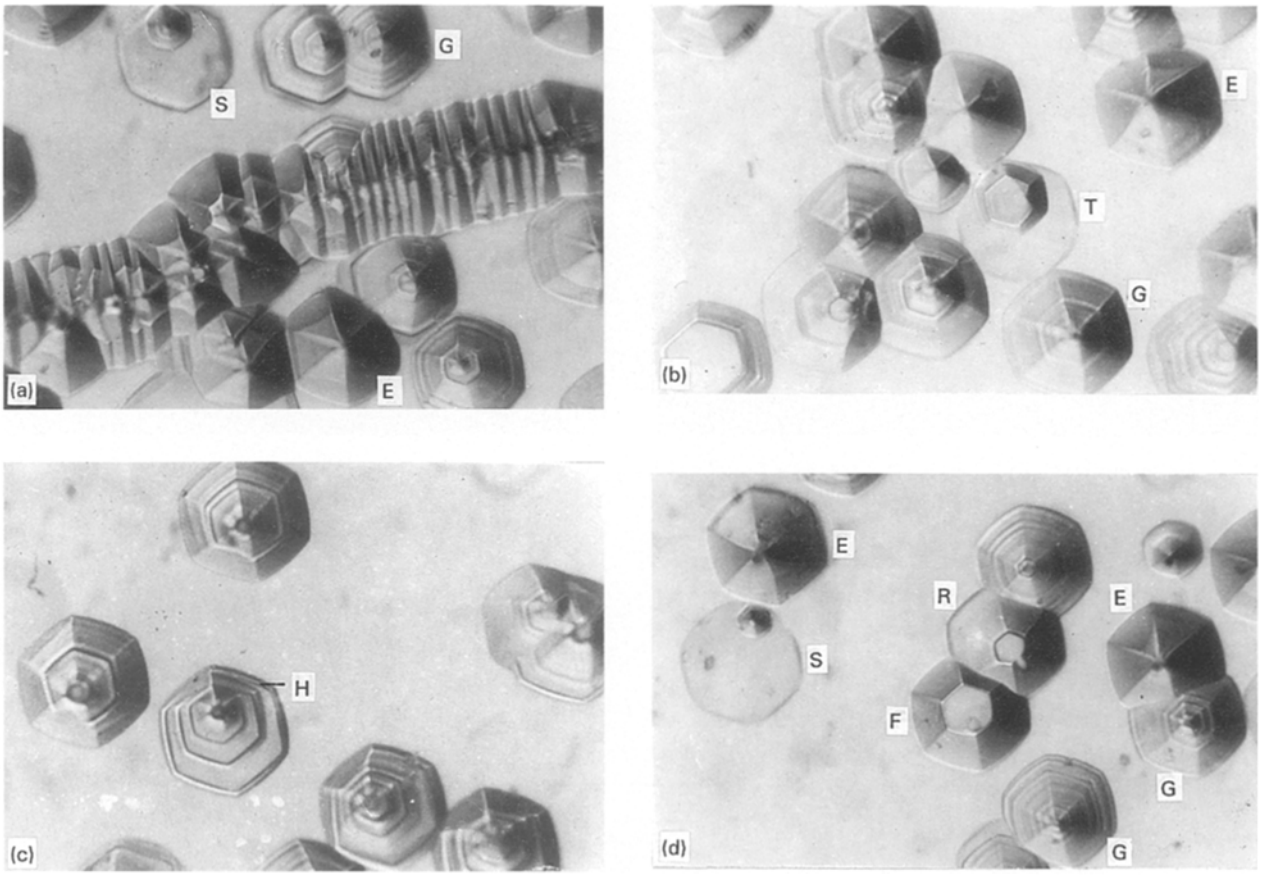

Figure 6(a) Row of etch pits along a lineage boundary on (0 0 0 1) face. Notice the formation of centred point bottomed hexagonal pits at E, closely spaced out regularly terraced and centred pits as at G, point-bottomed hexagonal pit within a flat-bottomed one with different geometrical centres as at S (etchant H_3PO_4 at 120 °C for 30 min). (× 480). (b) A habit (0 0 0 1) face etched in H_3PO_4 at 120 °C for 30 min. Notice the formation of smooth centred point-bottomed hexagonal pits as at E, closely spaced but regularly terraced pits as at G and one tiny point-bottomed hexagonal pit within flat-bottomed hexagonal pits as at T. (× 480) (c) Eccentric hexagonal pits with widely spaced terracings as at H on (0 0 0 1) habit face etched in H_3PO_4 at 120 °C for 30 min. (× 480) (d) Etch patterns on (0 0 0 1) habit face etched in H_3PO_4 at 120 °C for 30 min displaying formation of closely spaced but regularly terraced and centred pits as at G, smooth, centred flat-bottomed hexagonal pit with a beak as at R, tiny point-bottomed pit within a large flat-bottomed pit as at S and smooth flat-bottomed pits as at F. (× 480)

flat-bottomed pit away from its geometrical centre in which there is one more tiny point-bottomed pit, again with its centre not coinciding with the centre of either of the two flat-bottomed ones (as at T in Fig. 6(b)).

Terracing of etch pits has been discussed by Sangwal [16]. The application of bunch formation has been explained to give rise to terracings of etch pits [17]. Formation of terraced etch pits on the (0 0 0 1) planes of hexagonal materials, where the planes revealed by etching form an open figure, has been attributed to the consequence of the structure of the exposed plane [18, 19]. Another mechanism of the formation of terraced etch pits, involving variations in the concentration of impurities segregated at dislocations has also been suggested to be operative [20].

Since the etching of (0 0 0 1) planes of $SrFe_{12}O_{19}$ display terraced pits in combination with smooth pits, the authors are inclined to suggest that the terracing in the present case may arise due to the presence of impurities. The situation is explained in a schematic diagram of Fig. 7(a–d). The presence of impurity segregation affects the rate of nucleation of an etch pit along a linear defect. In case the impurity is such as to slow down the dissolution on account of its poor solubility, the rate of etch pit nucleation will be high only until an impurity precipitate is encountered (see Fig. 7(b)) and obviously, thereafter, the nucleation rate will fall. During the time the nucleation rate is low, the step formed during the period of high nucleation rate will advance away from the linear defect. When the impurity precipitate is removed as a result of either its own dissolution or by dissolution around it, the nucleation rate will increase. A repetition of this process will give rise to a terraced pit as explained by the schematic diagram in Fig. 7(b). Experimental evidence in support of this mechanism has also been reported in the case of (1 0 0) surfaces of LiF crystals [21].

In case the linear defect does not encounter an impurity and are normal to the surface of observation, a smooth, centred pit is expected as explained by the schematic diagram of Fig. 7(a). However, if the linear defect meets the impurities at regular intervals, a centred and regularly terraced pit with regular spacings is expected (see Fig. 7(b)). In the event that the linear defect meets impurities at irregular intervals, on account of its non-uniform segregation, one expects pits with irregularly spaced terracings but geometrically centric (see Fig. 7(d)). A linear defect inclined to the surface of observation encountering impurities at regular intervals should result into an eccentric and non-uniformly terraced pit (Fig. 7(c)).

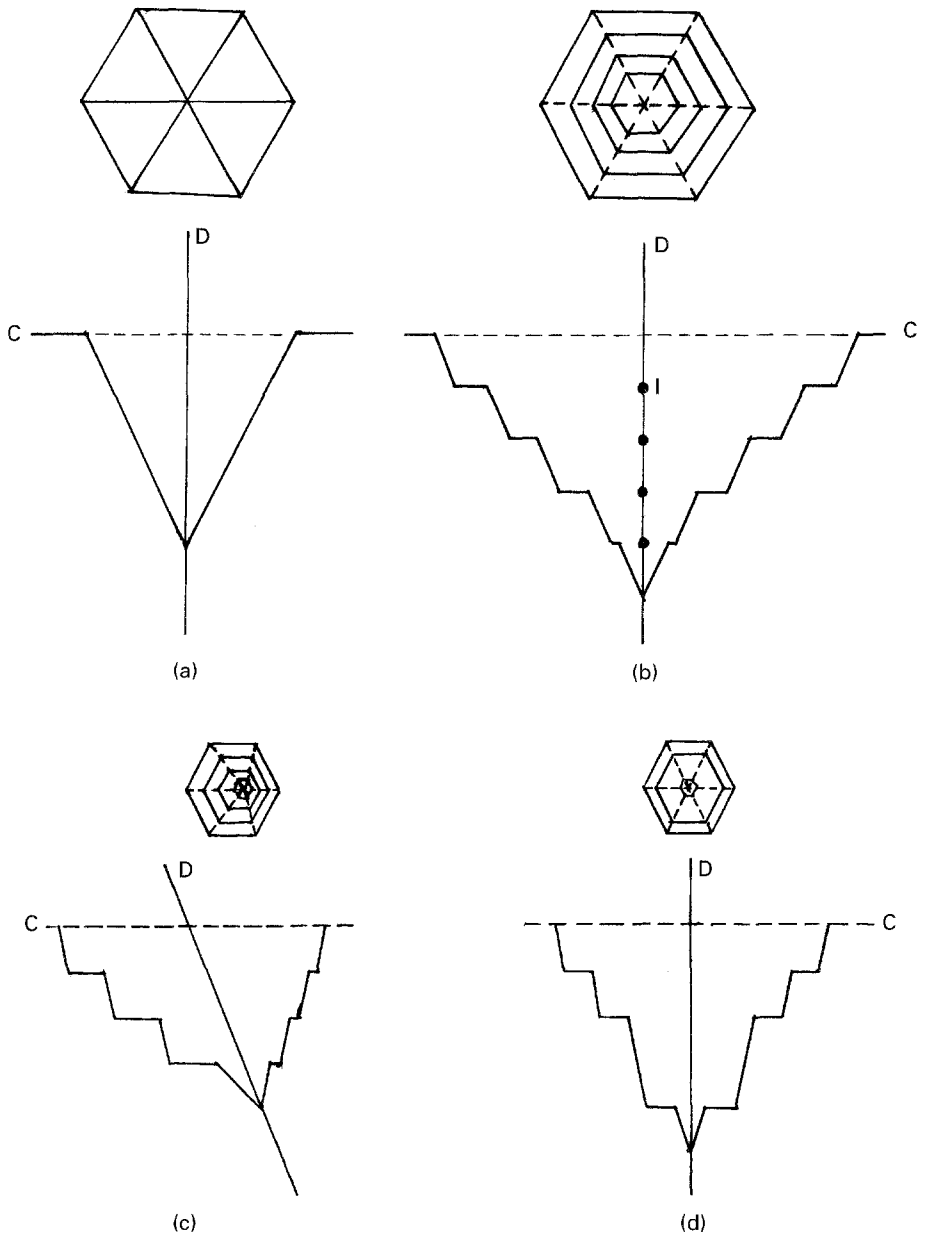

Figure 7(a, b, c, d) Schematic diagrams explaining the formation of hexagonal pit with smooth planes along a linear defect (a), uniformly and non-uniformly terraced pit due to etching of impurity segregation (b, c, d).

3.7. Stepped dislocations and bending of dislocations

In the etch patterns of (0 0 0 1) planes of $SrFe_{12}O_{19}$, one finds several examples of a smaller point-bottomed pit within a large flat-bottomed one. This could be attributed to the presence of stepped dislocations inside the crystal as explained in the schematic diagram of Fig. 8(a). The thin solid line in the schematic diagram marked D_1D_2 is a stepped dislocation which runs perpendicular to the surface for some depth in the body of the crystal, takes a turn parallel to the (0 0 0 1) surface and again turns in a direction perpendicular to the surface. If such a dislocation is etched, the profile of the pit first obtained will be ABC as in Fig. 8(a). However, if the etching continues, this initially nucleated pit will start getting flat and a new tiny pit will start emerging within a flat-bottomed pit at a point displaced from the geometrical centre of the flat-bottomed pit. Further etching will further flatten the initially nucleated pit (ABC) and increase the dimensions (both laterally as well as in depth) of the smaller displaced point bottomed pit. The profile of the pit will be of the type $A_2B_2C_2$, resulting in etch patterns of the type shown in Fig. 8(a). This explains the formation of pits of the type marked S in Fig. 6(a, d).

If the dislocation gets bent twice, we find two flat-bottomed pits (a smaller flat-bottomed pit within a bigger flat-bottomed pit with different geometrical centres) and a tiny point-bottomed pit with its nucleation centre displaced from the geometrical centres of either of the two flat-bottomed ones (as is seen in Fig. 6(b) marked T) and explained by the schematic diagram of Fig. 8(b). In case the dislocation normal to the surface gets bent parallel to the surface, say at the point slightly above D, we should be able to get only a flat-bottomed pit (see Fig. 9(a)). However, if the dislocation initially normal to the surface does not get bent exactly parallel to the surface (a situation shown in Fig. 9b) we expect a flat-bottomed pit with a beak (see R in Fig. 6(d)). In view of the observations made here and the explanations offered, we are inclined to

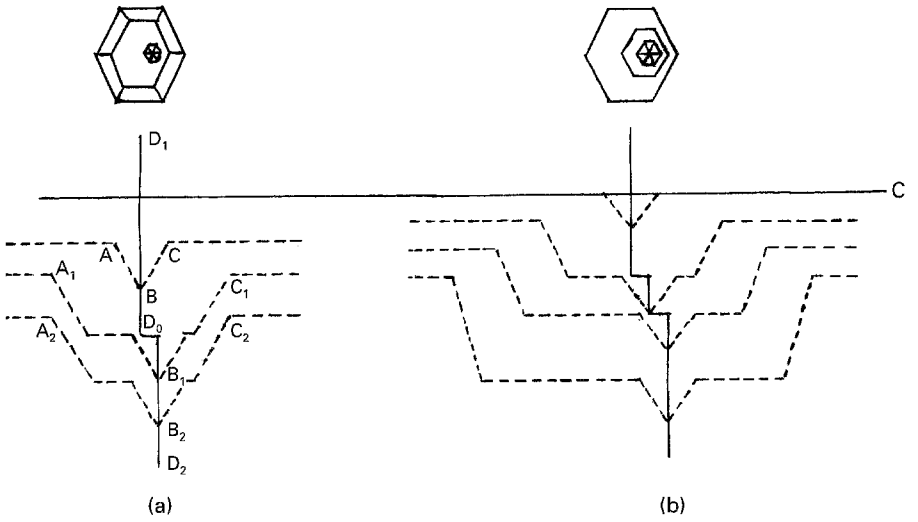

Figure 8(a, b) Schematic diagram explaining the structure of pits along stepped dislocations.

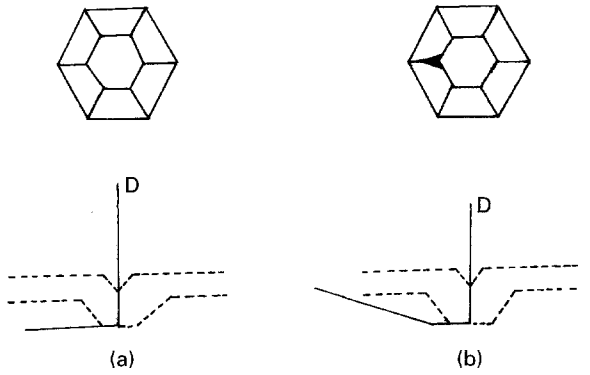

Figure 9(a, b) Schematic diagrams explaining the formation of a flat-bottomed pit at a dislocation bent parallel to the surface (a) and a flat-bottomed pit with a beak at a dislocation not bent exactly parallel to the surface (b).

suggest that there are inclined, bent and stepped dislocations in flux-grown $SrFe_{12}O_{19}$ crystals. If this is true, one should also be able to record mismatching of some etch pits on the two matched surfaces, as explained by Faust [18].

3.8. Etching of (0 0 0 1) cleavages in HCl

(0 0 0 1) Cleavages when etched in 37% HCl at 100 °C for 10 min also produce hexagonal pits. On successive etching the point-bottomed pits persist with increased dimensions and depth, thereby suggesting their formation at the points of emergence of linear defects (dislocations). When matched pairs are etched in this etchant, a perfect correspondence in regard to size, position and shape of etch pits is usually obtained on the two matched halves. This supports the conclusion drawn from the successive etching experiments.

3.9. Etching of matched cleavage in dissimilar etchants

It is interesting to note that when one of the cleavages is etched in 85% H_3PO_4 and matched half is etched in 37% HCl, most often perfect matching of the etch patterns is obtained. This observation suggests that both H_3PO_4 and HCl are able to reveal the existence

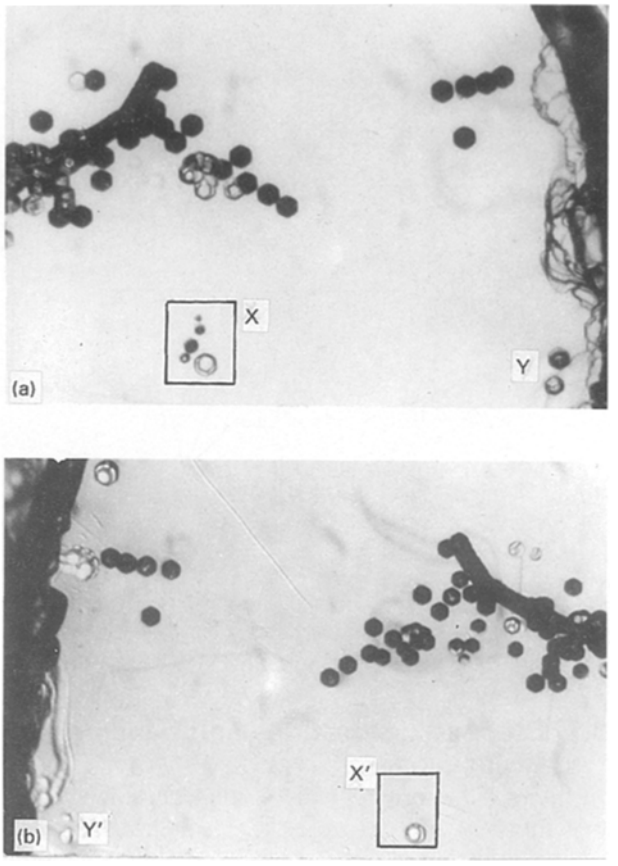

Figure 10(a, b) Mismatching of etch patterns on two matched (0 0 0 1) cleavages etched in (a) 37% HCl at 100 °C for 10 min, (b) 85% H_3PO_4 at 120 °C for 25 min. (× 120)

of same type of dislocations. There are, however, examples of deviations from perfect matching (mismatching) which are observed occasionally. Fig. 10(a, b) offers such an example wherein one of the cleavage faces is etched in 37% HCl at 100 °C for 10 min. and its matched half is etched in 85% H_3PO_4 at 120 °C for 25 min. A close examination of these two matched cleavage halves reveal mismatching at some specific sites. Some of the matched regions are (X and X') depicted at a higher magnification in Fig. 11(a, b) which shows that the etch patterns within these regions do not match on the cleaved halves (mismatching).

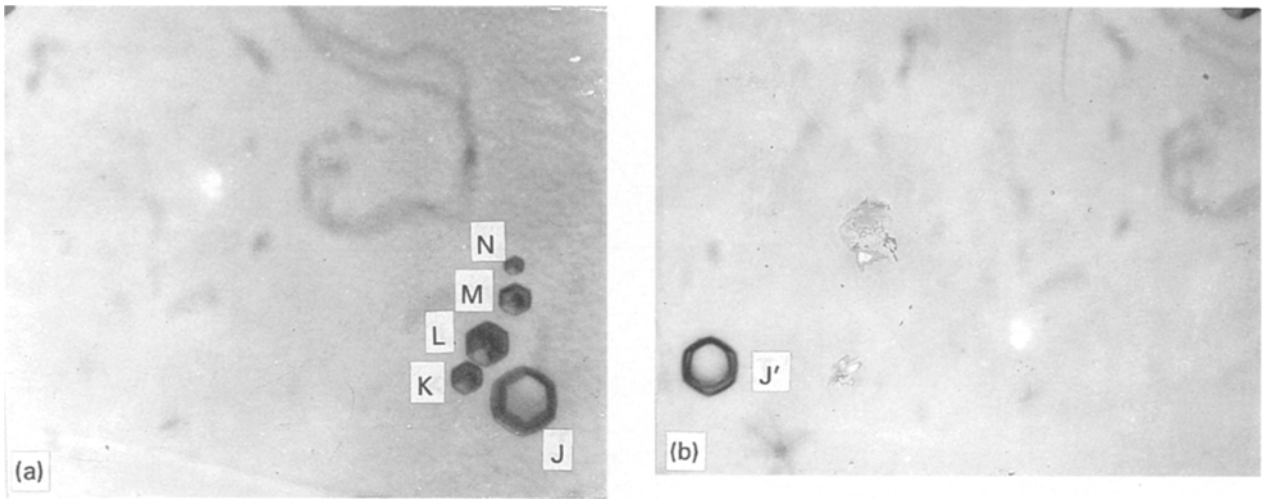

Figure 11(a, b) Regions marked X and X′ of Fig. 10(a) and (b) shown at a higher magnification depicting the mismatching and varying sizes of point-bottomed pits on one of the cleavages (see (a)). (× 240)

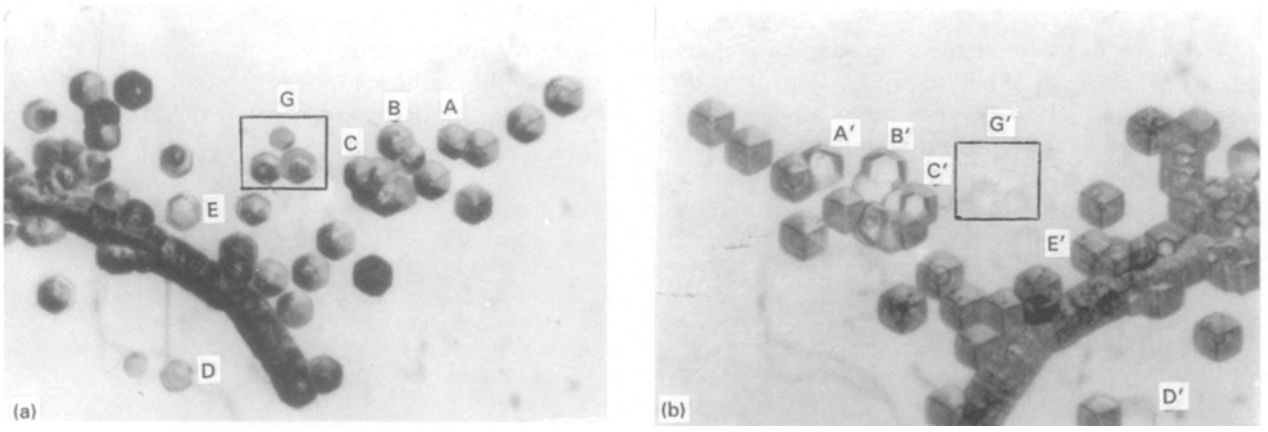

Figure 12(a, b) Regions of Fig. 10(a) and (b) at a higher magnification identifying mismatching of etch patterns.

One notices that corresponding to one-flat bottomed pit marked J in Fig. 11(a), there is a corresponding flat-bottomed pit J′ in Fig. 11(b). Such an unusual correspondence of flat-bottomed pits on the two matched halves is attributed to the presence of an impurity, as already explained in a schematic diagram of Fig. 4(a, b). Corresponding to the rest of the four pits marked as K, L, M, N in Fig. 11(a), there are no pits on the matched half of Fig. 11(b). Besides this mismatching, one also finds that these pits are of different sizes. The difference in the sizes including lateral dimensions and depth of pits K, L, M, N is attributed to their nucleation at different stages of etching. This situation is explained in the schematic diagram of Fig. 13(a, b, c, d). Here C represents the line of cleavage whereas A and A′ represent the corresponding planes on the two matched halves. D_3 is a thick solid line representing a dislocation line going right through the entire body of the crystal. D_2 is a dislocation which gets bent somewhere just below layer 1A. D_1 gets bent far more away from the cleaved plane. Considering that etching continues till the plane marked 3A and 3A′ is reached on either side of the cleavage plane, we obviously expect not only pits of different sizes on the cleavage half marked by As but also mismatching because corresponding to dislocations D_1 and D_2, there will not be any pit on matched half marked by As. The schematic diagram of Fig. 13(a, b) suggests a situation when the flat bottomed pits such as J and J′ should get washed off where as the pits K, L, M, N increase in their lateral dimensions and depth, if the cleavage planes of Fig. 11(a, b) are etched for a prolonged period. This is what was actually observed in the fourth stage of etching (i.e. total etching time of 2 and 1 h for cleavage planes of Fig. 10(a, b), respectively). Striking examples of several such mismatchings are noticed in the etch patterns formed in the upper half of Fig. 10(a, b), which are shown at a higher magnification in Fig. 12(a, b). Some of the mismatchings may be cited here as examples of situations that are expected from Fig. 13 (see D_4). Examples of flat-bottomed pits on one cleavage corresponding to point-bottomed pits on the matched cleavage (see a group of three point-bottomed pits within the rectangle marked G and also pits marked A, B, C, D, E is Fig. 12(a) corresponding to a group of three flat-bottomed pits marked G′ and A′, B′, C′, D′, E′ in Fig. 12(b), respectively. Most of the etch patterns

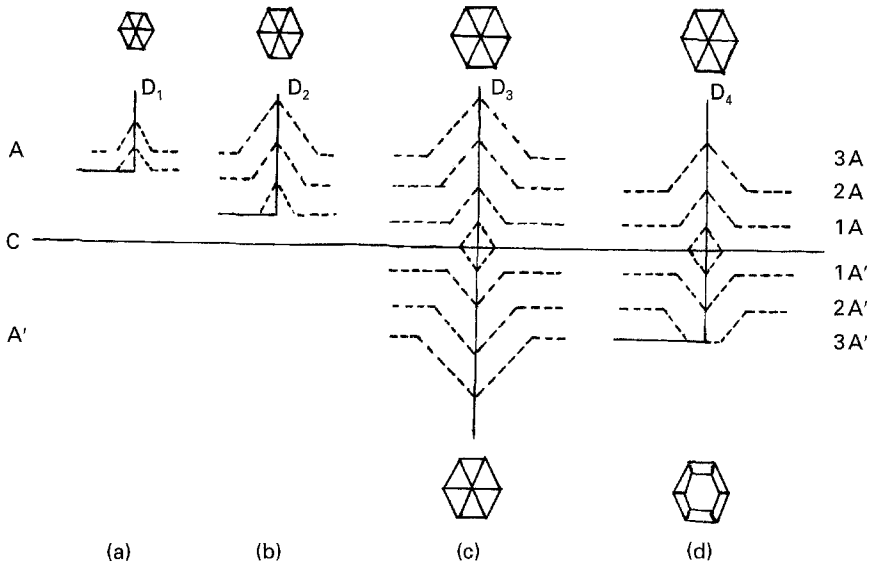

Figure 13(a, b, c, d) Schematic diagrams explaining the mismatching of etch patterns of Figs 10, 11 and 12 due to the presence of bending dislocations.

otherwise indicate matching on the two cleaved planes. The former situation is clearly explained by Fig. 13 (dislocation line D_4). In this case, the crystal is cleaved such that the dislocation line penetrates deep down the upper cleavage plane whereas it gets bent very near to the cleaved surface shown in the lower half below C. If etching continues, say, until 3A in the upper half and 3A′ in the lower half, one should expect a point-bottomed pit on one cleavage corresponding to a flat-bottomed pit on the matched cleavage.

4. Conclusions

1. The results of successive etching, etching of matched (0 0 0 1) cleavages and etching of a grain boundary establishes 85% H_3PO_4 at 120 °C and 37% HCl at 100 °C as dislocation etchants for $SrFe_{12}O_{19}$.

2. The terracing of hexagonal etch pits are attributed to the segregation of impurities, uniformly or non-uniformly along dislocations.

3. The eccentric hexagonal etch pits are suggested to originate at the inclined dislocations.

4. Small point-bottomed pits within larger flat-bottomed ones with their different geometrical centres, a short etch channel originating from the centre of a flat-bottomed pit, mismatching of point-bottomed pits on the matched cleavage planes, point-bottomed pits on one cleavage plane having flat-bottomed pits corresponding to them on the matched cleavage plane, are attributed to stepped and bending dislocations in strontium hexaferrites.

5. Point-bottomed pits of different sizes on one cleavage plane bearing no correspondence on the matched cleavage plane are attributed to bending of dislocations at different layers resulting into the nucleation of etch pits at different stages of etching.

6. Occasional correspondence of flat bottomed pits on matched cleavage planes and suggestive of etching rates different from elsewhere on the surface are attributed to the presence of impurity inclusions which are retained on both the cleavage planes.

Acknowledgement

One of the authors (S.B.) is thankful to the CSIR, New Delhi, for the award of a Research Associateship.

References

1. O. KUBO, T. IDO and H. YOKOYAMA, *IEEE Trans. Magn.* **18** (1982) 1122.
2. K. HANEDA and A. H. MORRISH, *ibid.* **25** (1989).
3. S. RINALDI and F. LICCI, *ibid.* **20** (1984).
4. G. TURILLI, F. LICCI and S. RINALDI, *J. Magnetism & Magnetic Mater.* **59** (1986) 127.
5. LIU JIZHE, *J. Mater. Sci. Mauking Univ.* (1980) 25.
6. S. AMELINKX, *Phil. Mag.* **1** (1956) 269.
7. A. SAGAR and J. W. FAUST, *J. Appl. Phys.* **38** (1967) 482.
8. *Idem., ibid.* **38** (1967) 2240.
9. M. S. JOSHI, M. A. ITTYACHEN and P. N. KOTRU, *Pramana* **10** (1978) 601.
10. M. S. JOSHI, P. N. KOTRU and M. A. ITTYACHEN, *Amer. Minerol.* **63** (1978) 744.
11. BONTINCK, *Phil. Mag.* **II** (1957) 561.
12. I. V. K. BHAGWAN RAJU, T. BHIMA SANKARAN and K. G. BANSIGIR, *J. Appl. Phys.* **40** (1969) 4668.
13. V. HARIBABU and K. G. BANSIGIR, *ibid* **40** (1969) 4306.
14. M. S. JOSHI and M. A. ITTYACHEN, *Ind. J. Pure Appl. Phys.* **7** (1969) 678.
15. M. S. JOSHI and R. K. TAKU, *J. Gemmol.* **13** (1972) 13.
16. K. SANGWAL in "Defects In Solids", edited by S. Amlinckx and J. Nihoul, vol. 15 on "Etching of crystals – theory, experiment and application" (North Holland Publications, Amsterdam, 1987).
17. K. SANGWAL and G. ZANIEWSKA, *J. Mater. Sci.* **19** (1984) 1131.
18. J. N. FAUST, in "The surface chemistry of metals and semiconductors", edited by H. C. Gatos (Wiley Publications, New York, 1960) p. 151.
19. H. C. GATOS, in "Crystal growth and characterization", edited by R. Ueda and J. B. Mullin (North Holland Publications, Amsterdam, 1975) p. 313.
20. J. J. GILMAN, in "The surface chemistry of metals and semiconductors", edited by H. C. Gatos, (Wiley Publications, New York, 1969) p. 172.
21. J. J. GILMAN, W. J. JOHNSTON and G. W. SEARS, *J. Appl. Phys.* **29** (1958) p. 747.

Received 22 December 1993
and accepted 20 November 1995